Monte Carlo Simulation of Sunlight Transport through Solar Trees – a New Paradigm for Improving Sunlight Capture Efficiency

Navni N. Verma and Sandip Mazumder

The Ohio State University

Abstract

Solar photovoltaic (PV) cells arranged in complex 3D leaf-like configurations—referred to as a solar tree—can potentially collect more sunlight than traditionally used flat configurations. It is hypothesized that this could be because of two reasons. First, the 3D space can be utilized to increase the overall surface area over which the sunlight may be captured. Second, as opposed to traditional flat panel configurations where the capture efficiency decreases dramatically for shallow angles of incidence, the capture efficiency of a solar tree is hampered little by shallow angles of incidence due to the 3D orientation of the solar leaves. In this paper, high fidelity Monte Carlo simulation of radiation transport is conducted to gain insight into whether the above hypotheses are true. The Monte Carlo simulations provide local radiation flux distributions in addition to global radiation flux summaries. The studies show that except for near-normal solar incidence angles, solar trees capture sunlight more effectively than flat panels—often by more than a factor of 5. The Monte Carlo results were also interpolated to construct a daily sunlight capture profile both for mid-winter and mid-summer for a typical North American city. During winter, the solar tree improved sunlight capture by 322%, while in summer the improvement manifested was 57%.

Keywords: sunlight capture, solar energy, solar tree, photovoltaic; Monte Carlo simulation, computational modeling

Introduction

Of the technologies available to utilize sunlight, solar photovoltaic (PV) energy conversion that directly converts solar energy to electricity has been in existence for almost four decades. Solar PV power is arguably the most mature amongst competing solar energy technologies. Significant progress has been made in increasing the conversion efficiency of solar cells—in large part due to the development of novel semiconductor materials and nanostructures.

Despite significant progress in the conversion efficiency of solar PV cells and dramatic reduction in their manufacturing cost in the past few years, use of solar PV technology has been limited to areas of "abundant" sunshine. The solar constant is approximately 1362 W/m^2 (Lee, 1978), which is the average irradiation on the earth without atmospheric attenuation and tilt effects. The actual average solar irradiance in the United States is about 185 W/m^2 compared to a global average of 170 W/m^2 (NREL, 2014). The numbers just cited are average annual values after accounting for atmospheric attenuation and both day and night. However, the majority of the solar energy in the US is concentrated in the states of Arizona, Nevada, and California (NREL, 2014). The entire north-eastern part of the country, which has the highest population density, has cloudy climate and poor sunshine, especially during the winter season. While it is true that poor sunshine, cloudy climate, and short days are all factors that adversely affect solar cell performance, investigations into how and why these factors adversely affect the performance of solar cells, may ultimately result in better utilization of solar energy.

Figure 1 shows the solar insolation at Columbus, which is located on the 40^oN latitude. The insolation is defined as the theoretical incident solar flux on a flat surface without accounting for atmospheric attenuation of the sunlight. Its peak value is the solar constant, *i.e.*, 1362 W/m^2. The insolation is shown on two different surfaces: one that is north-facing and at an

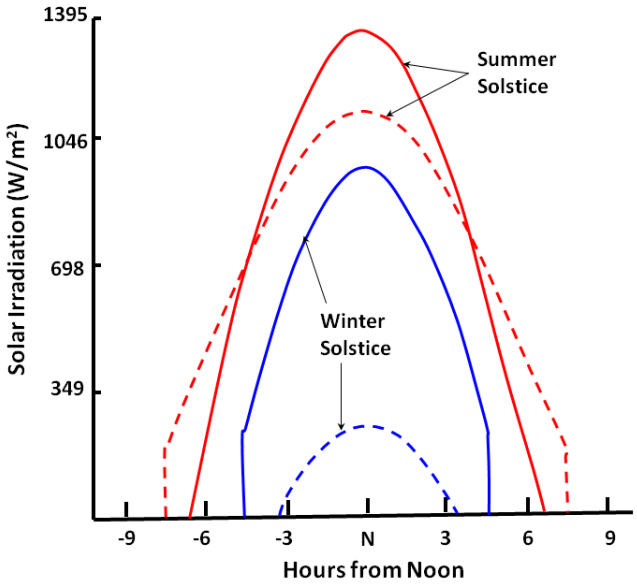

Figure 1. Instantaneous solar insolation at 40°N latitude on summer and winter solstice. The solid lines are for a south-facing surface inclined at 15.7° with the ground, while the dotted lines are for a north-facing surface inclined at 15.7° with the ground. The data were generated using relationships available in Lee (1978).

angle of 15.7° with the ground, and another that is at the same angle with the ground, but south-facing. As expected, during the summer solstice, the peak insolation reaches a maximum on a south-facing surface, and the maximum is very close to the solar constant. However, it is worth noting that a north-facing surface, although it receives less peak irradiation than a south-facing surface, receives radiation over a longer period of time. In fact, the total radiation received (area under the curve) by a north-facing surface is larger than a south-facing surface. These data would indicate that in a single day, solar cells facing northward should produce as much, if not more, electricity compared to solar cells that face southward. In reality, however, it is observed that solar cells facing north are significantly less productive than ones that face south (Komp, 2001). This discrepancy begs an explanation.

First, Lambert's cosine law states that the normal radiation flux to any surface is proportional to the cosine of the angle between the incident radiation and the surface normal to

the surface. This implies that for grazing angles of incidence, the sunlight captured will be minimal since cosine of an angle close to 90^o is very small. Secondly, solar PV cells are comprised of a stack of doped semiconductor films that utilize the incident photons to generate free electron and hole pairs. This delicate structure is usually covered on the top by a sheet of glass to protect it from the environment. Any sunlight striking the solar PV cell has to first pass through the glass cover prior to being utilized. The measured directional reflectivity of a glass sheet painted black on one side to eliminate multiple reflections within the sheet is shown in Fig. 2. The data shown in Fig. 2 are for monochromatic green light. The angle of incidence is measured from the normal to the glass surface. The figure shows that the reflectivity increases

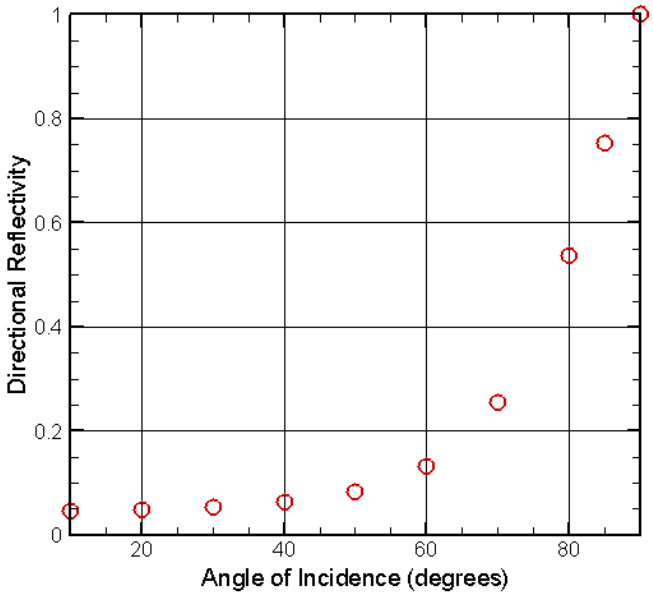

Figure 2. Measured directional reflectivity of a glass sheet for green light. The glass sheet was painted black on one side to eliminate multiple reflections within the glass. The measured data are extracted from Modest (2013), and also agrees with theoretical predictions using electromagnetic wave theory, as shown in the same reference.

sharply beyond an angle of incidence of 60^o. In fact, from 60^o to 70^o the reflectivity increases by approximately a factor of two. While it is true that a north-facing surface receives more net solar radiation during mid-summer than a south-facing surface (Fig. 1), much of the radiation on a

north-facing surface is at near-grazing angles of incidence, and therefore, fails to penetrate the glass cover. On account of the afore-stated two reasons, solar PV cell vendors insist that the solar panels should be installed such that they face direct sunlight. The problem may be circumvented partially by using low refractive index glass and/or tailoring its optical properties, such as in so-called solar glass or nano-patterned glass (Verma et al., 2011). However, such modifications primarily alter the normal reflectivity, and not the reflectivity at grazing angles, as predicted by electromagnetic wave theory (Modest, 2013). Additionally, these modifications increase manufacturing expenses and are not viable since cost is already a major concern for PV technology. In large-scale solar PV "farms" operated by utility companies, the sun is often tracked by a heliostat, and the inclination of the solar panels is changed so that the angle of irradiation is almost always normal. Such an approach, however, is impractical for solar panels installed on rooftops or walls.

In this study, it is hypothesized that trees are effective at capturing sunlight because of two reasons. First, their leaves are oriented at almost random angles to the solar irradiation. Thus, while some of the leaves may be encountering grazing angles, others are encountering almost normal angles of incidence at the same instant of time. Second, since trees grow vertically, they are able to utilize the entire 3D space rather than just the 2D footprint to collect sunlight. Thus, the area over which sunlight is collected is very large. These hypotheses are substantiated by research on solar radiation absorption by trees which show that the absorption is strongly dependent on the solar zenith angle and the leaf area index (same as area ratio in this study) (Brown and Pandolfo, 1969; Mann et al., 1979; Bartelink, 1998; Perttunen et al., 1998; Abraha and Savage, 2010).

The idea of placing solar cells in random orientation to mimic leaves of a tree led to the

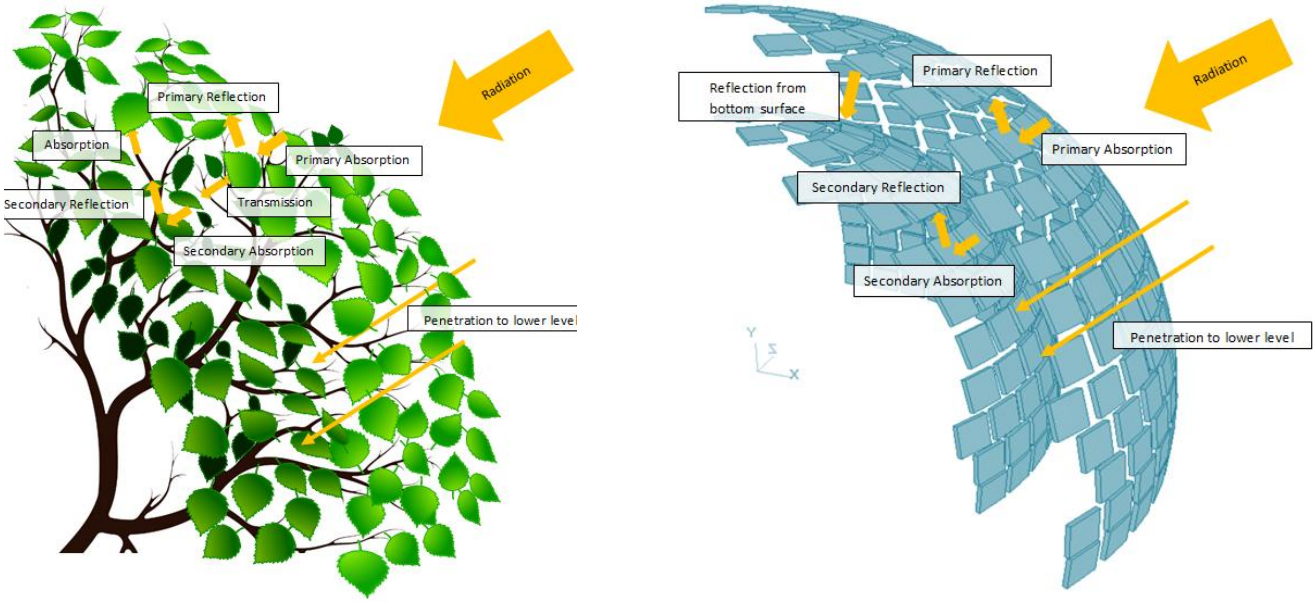

(a) *(b)*

Figure 3. Radiation flow pathways in (a) in actual tree, and (b) solar tree

so-called "solar tree," a schematic illustration of whose working principle is shown in Fig. 3. There is adequate preliminary proof available to suggest that solar trees have strong potential. In 2010, Aidan, a seventh-grader from New York and winner of the Young Naturalist Award sponsored by the American Museum of Natural History, embarked upon designing, building, and testing a solar tree similar to the one proposed in this study. Although Aidan's research does not quantify the gains provided by a solar tree over a conventional flat solar panel array, states (AMNH, 2011): "*The tree design takes up less room than flat-panel arrays and works in spots that don't have a full southern view. It collects more sunlight in winter*." A Japanese group recently also conducted research on a similar design (Asai and Toshiaki, 2010) in which they placed solar leaves using a Fibonacci sequence on a single-stemmed solar tree, and reported significant gains over conventional unidirectional solar panels. However, their findings are purely model-based, and it is not clear what model was used. Furthermore, their model neglects shadowing effects. The city of Vienna introduced solar trees in 2007 for street lighting

(Burgermeister, 2007). The preceding examples clearly point to the fact that a treelike configuration is, perhaps, worth considering for efficient sunlight capture, especially in locations where winters dominate. However, none of the aforementioned efforts has delved deep into the science behind radiation transport, nor have they performed systematic study of key variables. The success of these preliminary designs has generally been attributed to reasons that are plausible but unconfirmed. In this study, we conduct high-fidelity Monte Carlo simulations of solar radiation transport with the goal to test the hypotheses stated earlier, and to elucidate the exact reasons why 3D solar trees, as opposed to flat unidirectional solar panels, may or may not improve sunlight capture.

Mathematical Model and Solution Method

For the purposes of this study, air may be assumed to be a non-participating medium, i.e., one hundred percent transparent to radiation. This is because for the length scales under consideration—few meters—the optical thickness propagated by a photon is extremely small (Modest, 2013). In the absence of a participating medium, the spectral (at any wavelength, λ) radiation flux on a surface, i, is a result of the net emission by the surface and the net incoming energy. It may be written as (Modest, 2013):

$$Q_{\lambda,i} = q_{\lambda,i}A_i = \varepsilon_{\lambda,i}A_i E_{b\lambda,i} - \sum_{j=1}^{M} R_{\lambda,ij}A_j E_{b\lambda,j} \quad (1)$$

where M is the total number of boundary surface elements (or faces) with A_j being their surface areas. $\varepsilon_{\lambda,i}$ is the spectral emissivity, and $E_{b\lambda,i}$ is the spectral blackbody emissive power. The spectral radiation exchange matrix, $R_{\lambda,ij}$, the radiation energy of wavelength λ emitted by any surface j and collected (absorbed) by i after multiple reflections. Therefore, it includes any

reflected energy from surface i. In order to calculate the total radiation flux, Eq. (1) must be integrated over the entire spectrum, yielding

$$Q_i = q_i A_i = A_i \int_0^\infty \varepsilon_{\lambda,i} E_{b\lambda,i} d\lambda - \sum_{j=1}^{M} A_j \int_0^\infty R_{\lambda,ij} E_{b\lambda,j} d\lambda \tag{2}$$

The total emissivity of a surface is expressed in terms of its spectral emissivity using the following definition (Modest, 2013):

$$\varepsilon_i = \frac{\int_0^\infty \varepsilon_{\lambda,i} E_{b\lambda,i} d\lambda}{\int_0^\infty E_{b\lambda,i} d\lambda} = \frac{\int_0^\infty \varepsilon_{\lambda,i} E_{b\lambda,i} d\lambda}{\sigma T_i^4} \tag{3}$$

where T_i is the absolute temperature of surface i. Similarly, the total radiation exchange matrix may be expressed in terms of the spectral radiation exchange matrix using

$$R_{ij} = \frac{\int_0^\infty R_{\lambda,ij} E_{b\lambda,j} d\lambda}{\int_0^\infty E_{b\lambda,j} d\lambda} = \frac{\int_0^\infty R_{\lambda,ij} E_{b\lambda,j} d\lambda}{\sigma T_j^4} \tag{4}$$

Substituting Eqs. (3) and (4) into Eq. (2) yields

$$Q_i = q_i A_i = A_i \varepsilon_i \sigma T_i^4 - \sum_{j=1}^{M} A_j R_{ij} \sigma T_j^4 \tag{5}$$

Using the Kronecker delta function, Eq. (5) may be written as

$$Q_i = q_i A_i = \sum_{j=1}^{M} A_j \delta_{ij} \varepsilon_j \sigma T_j^4 - \sum_{j=1}^{M} A_j R_{ij} \sigma T_j^4 = \sum_{j=1}^{M} A_j (\delta_{ij} \varepsilon_j - R_{ij}) \sigma T_j^4 \tag{6}$$

The Monte Carlo method has found prolific use in the simulation of radiation transport for a variety of applications (Modest, 2013; Mazumder and Kersch, 2000). In essence, the Monte Carlo method is a statistical method, which is used to compute R_{ij}. In this method, photon bundles (or rays) are emitted from surfaces based on certain random number relations derived

from Planck's law and the cosine law. These photon bundles are then traced until they are completely absorbed. In the absence of a participating medium (i.e., fully transparent gas), photons need to be tracked only from surface to surface. Once the number of rays is tallied, the ratio of the number of rays absorbed by a surface j to the number of rays emitted by surface i denotes the radiation exchange matrix R_{ij} (Modest, 2013). The Monte Carlo method inherently accounts for any obstructions in the geometry and shadowing effects. In the Monte Carlo method, the combined statistics of all wavelengths is gathered and processed because what is of final interest is the total radiation flux, not the spectral radiation flux.

The starting point of the present computational study was a Monte Carlo code developed to simulate radiation transport in rapid thermal chemical vapor deposition reactors (Mazumder and Kersch, 2000). In recent years, the core ray tracing procedure has also been enhanced to drastically improve the computational speed (Mazumder, 2006). Some of the salient features of this code that are pertinent to this study are as follows:

- The code can trace rays through complex 3D geometries discretized using an unstructured mesh of arbitrary mesh topology.
- The spectrum is discretized using 60 bands (or wavelength intervals) based on a logarithmic scale. The number of bands was determined to be the optimum (from accuracy and computational efficiency standpoint) after extensive numerical experimentation.
- Surfaces can be diffuse, specular, or partially specular.
- Ray tracing is conducted using a state-of-the-art ray tracing algorithm, namely the Volume-by-Volume Advancement algorithm (Mazumder, 2006).

As discussed earlier, solar cells are covered with a glass sheet, whose reflectivity is not only dependent on wavelength and temperature but also on the angle of incidence. Using the Fresnel relationships, the directional reflectivity of glass can be derived, and is written as (Modest, 2013)

$$\rho = \frac{1}{2}\left[\left(\frac{n^2\cos\theta - \sqrt{n^2 - \sin^2\theta}}{n^2\cos\theta + \sqrt{n^2 - \sin^2\theta}}\right)^2 + \left(\frac{\cos\theta - \sqrt{n^2 - \sin^2\theta}}{\cos\theta + \sqrt{n^2 - \sin^2\theta}}\right)^2\right] \tag{7}$$

where ρ is the spectral directional reflectivity. Since the refractive index, n, is a function of both temperature and wavelength, the reflectivity is also a function of both temperature and wavelength. In Eq. (7), θ is the incident angle (i.e., the angle between the incident ray and the surface normal). The aforementioned Monte Carlo code was modified to incorporate this model. For the present study, the reflection from the glass surface was assumed to be diffuse. The nature of reflection from the glass cover is somewhat unimportant because any reflected energy is permanently lost. Therefore, it is the fraction of energy that is reflected and not its direction that is relevant. The wavelength dependent refractive index of glass was extracted from Palik (1997). The antireflective coating coupled with multiple reflections within the cavity between the top glass sheet and the antireflective coating allows negligible amount of radiation to exit the solar cell once it is transmitted through the topmost glass sheet. Therefore, the reflective property of the glass sheet is of primary significance.

Results and Discussion

Code Verification

Prior to conducting simulation of solar trees, the Monte Carlo code was first verified. This was done by comparing the results predicted by the Monte Carlo code against results computed using the view-factor method (an exact semi-analytical method) (Modest, 2013). Since the view-factor method can only be applied to relatively simple geometries with gray diffuse

walls, the simulations were conducted in a 3D bricklike geometry with gray diffuse walls of fixed temperature, as illustrated in Fig. 4. All walls were assumed to have an emissivity of 0.5. A 11x11x23 mesh was used to discretize the geometry. The view-factors between individual surface elements were computed using the contour integral method (Modest, 2013) with parametric representation of the surfaces (Mazumder and Ravishankar, 2012), and a 20-point

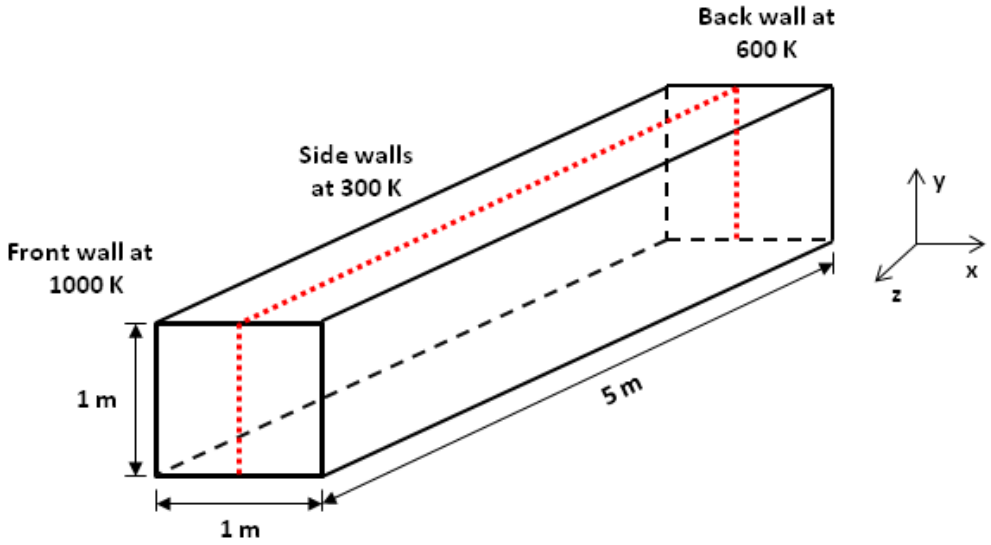

Figure 4. Geometry and boundary conditions for the test case used for validation study. The red dotted lines indicate paths along which the heat fluxes predicted by the two methods were compared.

Gaussian quadrature formula was used for evaluation of the resulting contour integrals. The Monte Carlo simulations traced 100×10^6 rays, and five ensembles were computed to enable calculation of the mean values and statistical errors (standard deviations), which were found to be less than 0.06% at any surface. Figure 5 shows the computed non-dimensional radiative heat flux along the paths on various walls that are shown in Fig. 4. The heat fluxes were normalized using $\sigma(T_H^4 - T_C^4)$, where T_H = 1000K and T_C = 300K were used in this particular case. All distances were normalized by the length of the channel (= 5 m). Clearly, the Monte Carlo method is able to reproduce exact analytical results almost perfectly. The error between the two methods

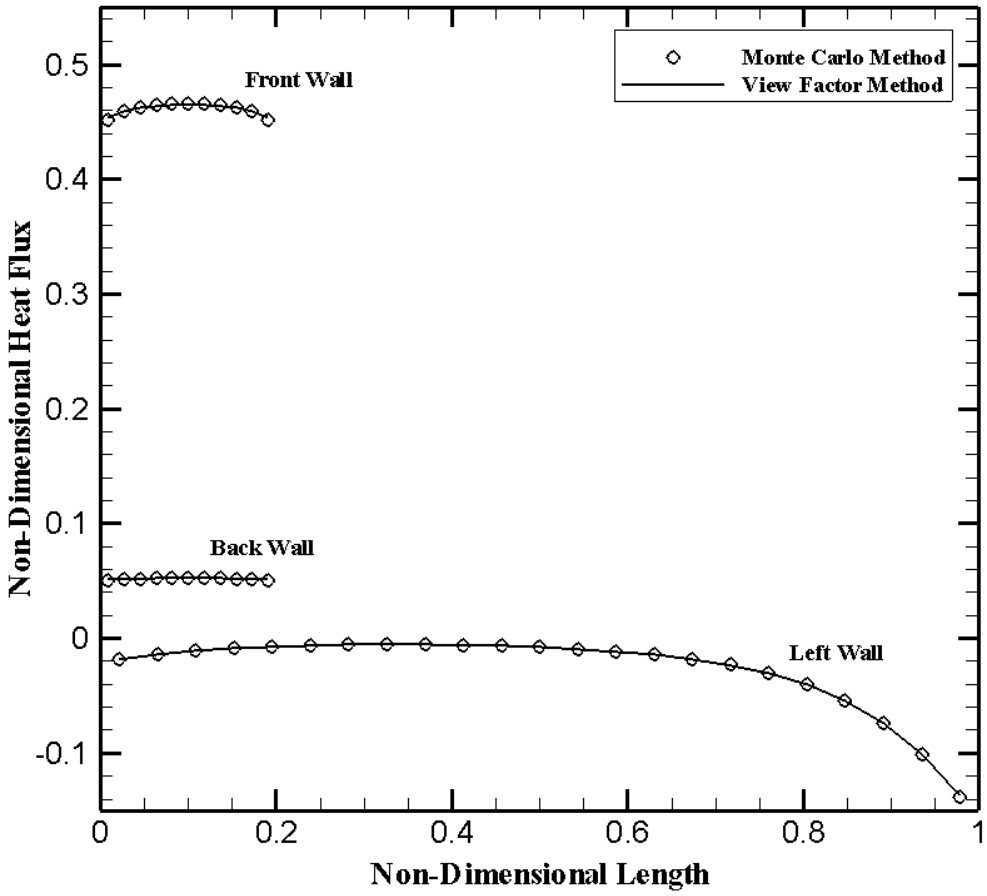

Figure 5. Comparison of non-dimensional heat fluxes computed on the various walls.

(view factor and Monte Carlo) was found to be less than 0.009% at any location. It is worth noting that the Monte Carlo method does not rely upon the specific rectangular features of the geometry considered in this verification study. Therefore, although this verification study does not conclusively prove the suitability of the Monte Carlo code for solar tree simulations, it does lend confidence to the execution of the algorithm used here and the underlying calculation procedure.

Monte Carlo Simulation of Solar Trees

Solar trees were virtually constructed by placing solar cells along the surface of a hemispherical contour, and half of a hemisphere was considered so that the polar angle (solar incidence angle, θ) could be varied from 0 to 90°. For the first set of simulations, only a single

layer of cells (leaves) were considered, as shown in Fig. 6. The nominal radius of the tree (hemisphere) was chosen to be R = 2 m, resulting in a footprint area of 6.283 m^2. Consistent with availability in the market (from Everbright Solar Inc.), individual solar cells (leaves) of dimension 6.5" × 6" were used. The backsides of the cells were assumed to be coated with a reflective alumina paint of reflectivity 93%. For a single-layer tree, the maximum total area of the leaves is the surface area of the half-hemisphere $(=\pi R^2)$. The footprint area of the same tree is that of half of a circle $(=\pi R^2/2)$. Therefore, the maximum area amplification possible by placing leaves in a 3D arrangement is a factor of 2. The ratio of the actual area of the leaves to the footprint area is henceforth referred to as the area ratio. The number of solar cells (leaves) was treated as a parameter in this study. For example, Fig. 6(a) illustrates a case where 384 leaves were used, resulting in a total capture area of 9.662 m^2, and an area ratio of 1.54. Two other area ratios were also considered in this study. Another parameter considered in this study is

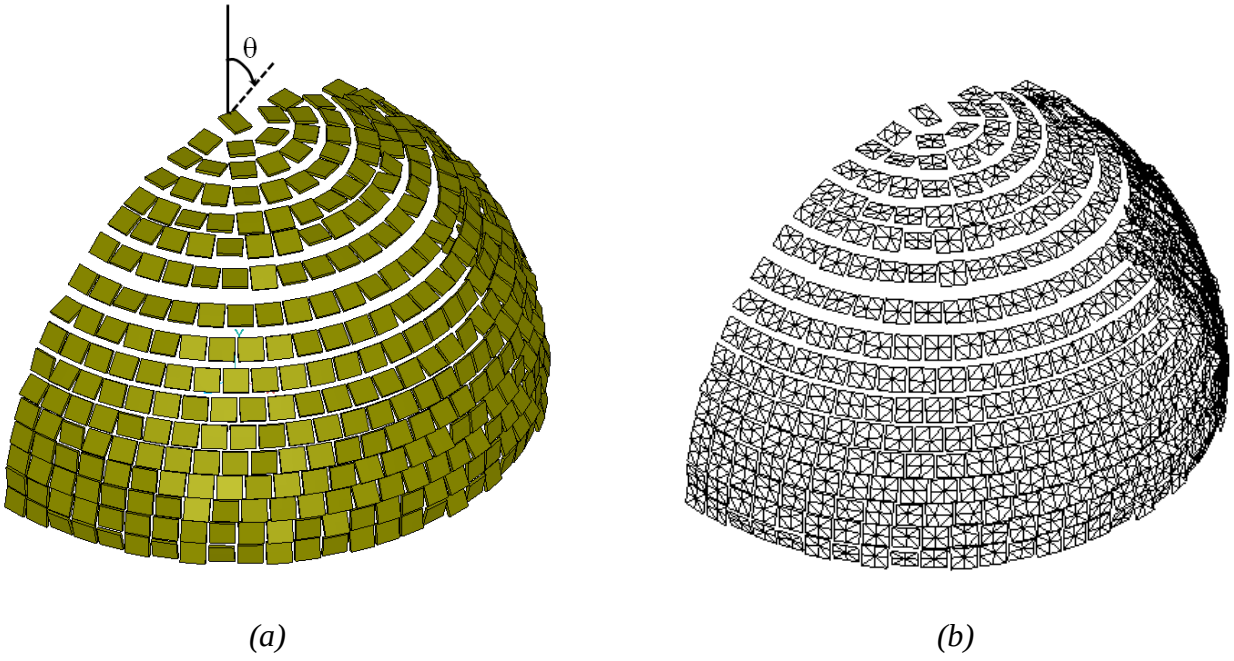

(a) *(b)*

Figure 6. Simulated single-layer solar tree with individual leaves (solar cells) tilted within the range ± 20 deg: (a) geometry and (b) mesh used for simulation.

the angle of the leaves (solar cells). Nominally, the cells were placed tangential to the hemispherical surface. However, since leaves of actual trees are oriented almost randomly, a similar idea was considered for the solar tree in which the solar cells were tilted randomly about their own axes within a prescribed range of angles. The effect of variation of these parameters will be discussed in subsequent sections.

Considering the complexity ensuing from the aforementioned parametric variations, one of the challenging aspects of this study is the development of an efficient algorithm for the creation of the geometry for the solar trees prior to Monte Carlo simulations. The commercial mesh generation software CFD-GEOM™ was used in the present study for mesh generation. This particular software allows interfacing with Python scripts that may be used for geometry creation and subsequent parametric variation of the geometry. Once the geometry is created by the Python script, it is automatically meshed by CFD-GEOM™. For the present study, a carefully designed Python script was written to accommodate all of the aforementioned geometric parameters, so that the mesh generation process became almost automatic. Figure 6(b) shows a typical surface mesh used for the present study. It is comprised of 12,376 triangular elements. As evident in Fig. 6(b), each leaf was discretized using 8-10 triangular elements so that the radiation flux on each leaf could be sufficiently resolved.

Subsequent to mesh generation, Monte Carlo simulations of radiation transport in the solar trees were conducted. The input solar flux used in these simulations was 1362 W/m^2 i.e., the solar constant. For each Monte Carlo simulation, 100×10^6 rays (or statistical samples) were traced. Also, for each case, five ensembles (five independent sets of 100×10^6 rays) were computed. This enabled computation of both the mean radiation fluxes as well as their standard deviations. Typically, with 100×10^6 rays, the standard deviations were found to be about

0.0425% of the mean values, indicating high statistical accuracy of the computed results. Each simulation required about 15 min of computational time on a high-end desktop computer. Figure 7 shows the computed radiation flux distribution for the case shown in Fig. 6. For this particular case, the solar incidence angle (θ) is 40°. It is seen that the local radiation flux depends not only on the solar incidence angle, but also on the tilt angle (orientation) of the individual leaves.

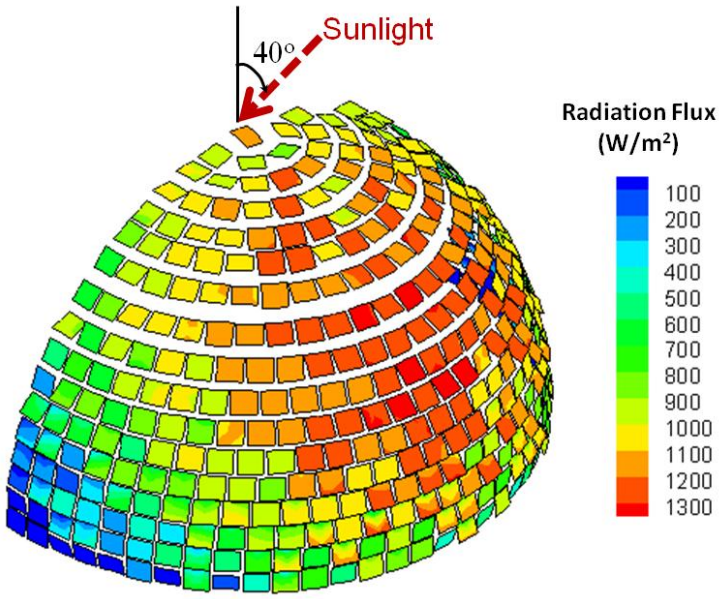

Figure 7. Computed radiation flux on a single-layer solar tree with 40^{o} solar incidence angle and leaf tilt angles ranging between ± 20 deg. The incident solar flux is 1362 W/m^2.

In order to delineate the implications of using a solar tree versus a flat panel, calculations such as those reported in the preceding paragraph were performed for several parametric variations. Since, this is a comparative study, the input solar flux (1362 W/m^2) has no bearing on the findings of this study. A flat panel refers to a solar panel without any curvature, and placed flat on the ground. For each case, the total (summed over all solar leaves) captured radiation flux was computed. The parametric variations that were considered are (a) angle of solar irradiation, (b) angle of tilt of the individual leaves, and (c) the area ratio. The results of these parametric studies are discussed next.

Effect of angle of solar irradiation. Six different solar irradiation angles (θ) ranging from 0 to 80° were considered. These angles represent inclinations of the sun during various times of the day and/or different seasons/latitudes. It is commonly referred to as the solar zenith angle. The incoming solar radiation was assumed to be collimated. This assumption is justified since the solid angle subtended by the sun on the earth is extremely small (see page 12 of Modest, 2013). Additional effects, such as atmospheric refraction, are not considered in this study. The total captured solar fluxes are tabulated in Table 1. As expected, for near-normal incidence ($\theta = 0^{\circ}$, 20°), flat solar panels capture more sunlight than a solar tree even if the capture area of the solar tree is 1.54 times that of the solar panel, i.e., area ratio of 1.54. However, at solar incidence angles of 40° or larger, solar trees capture more sunlight than flat panels. At shallow angles of incidence ($\theta = 80°$), a solar tree is found to capture 4-6 times more sunlight than a flat panel. Table 1 clearly shows that the gains provided by a solar tree far outweigh the losses since the losses are less than 80% while the gains are often in excess of 400%. Another important point to note is that a flat panel is far more sensitive to the solar irradiation angle than a solar tree. For example, for the case where the area ratio is 1.15, the captured solar flux by a flat panel ranges between 8275 W and 914 W—almost a factor of 9 variation. In contrast, for a solar tree, the variation is between 6111 W and 2154 W, *i.e.*, only a factor of 3. In other words, a solar tree is much more robust and reliable for capturing sunlight irrespective of geographic location, season, or time of day—the three factors that mainly affect the solar incidence angle.

Effect of tilt angle of leaves. The solar leaves were tilted from their baseline tangential positions to mimic leaves of a tree. Two different variations were considered: one in which the leaves were tilted randomly within and angle ranging from -20° to +20°, and another in which

they were tilted randomly between -40° and +40°. Random numbers were drawn and used within the aforementioned Python script for geometry creation to generate the tilted leaves. The tilting angles considered here were arbitrarily chosen, primarily with the goal to investigate if tilting of the leaves significantly alters the results. Based on the results reported in Table 1, it appears that excessive tilt is detrimental to the performance. The ±40° case consistently underperforms the capture efficiency of the other two cases. Essentially, at high angles of tilt, some of the radiation escapes through the gaps between the leaves. Furthermore, the radiation striking the leaves is often at grazing angles, and is not captured as effectively for reasons discussed earlier. When comparing the ±20° tilt case with the case with no tilt (0° tilt), the results are unpredictable. Both losses and gains are observed due to the ±20° tilt, implying that tilting of the leaves is not a necessary criterion to increase sunlight capture.

Effect of area ratio. One of the advantages offered by a solar tree over a flat panel is the amplification of the capture area due to the 3D placement of the leaves. From Table 1, it is clear that a larger area ratio results in more effective sunlight capture. For example, for area ratio equal to 1.15 and a solar incidence angle of 40°, flat panels perform better than solar trees. However, for the same solar incidence angle, increasing the area ratio to 1.54 results in reversal of this trend. In principle, it is possible to increase the area ratio even further—to the point where the solar tree captures more sunlight compared to a flat panel even for normal angles of incidence. However, this requires careful geometric design, as will be discussed in the section to follow.

The increase of the area, however, comes at an additional cost, and that may not always be desirable. Another way to compare a solar tree with a flat panel may be to consider a scenario in which both have the exact same capture area. In order to make such a comparison, the radiation captured by a flat panel was computed by multiplying the actual captured flux with the

area ratio. These fluxes are reported in Table 1 within parenthesis immediately below the reported values of the sunlight actually captured by the flat panel. If these fluxes are compared against the fluxes captured by a solar tree, it is found that solar trees provide substantial gains with irradiation angles greater than 40°. This implies that the gains manifested in a solar tree are not due to area amplification alone, but also due to the complex interactions between the radiation direction and the 3D placement of the leaves.

Effect of multiple layers of leaves. In the previous section, the highest area ratio considered is 1.54. In principle, it is possible to pack the leaves more closely in the outer layer, so that a higher area ratio is manifested. An alternative approach is to use a second layer of leaves underneath the first layer, such that this layer may capture some of the sunlight escaping through the gaps of the outer layer. The benefit of this approach is that an area ratio greater than 2 is possible. In an effort to investigate this idea, a second layer of 191 new leaves was added to the tree at a radius of 1.5 m, while still retaining the exact same leaf placement at the outer layer at 2 m radius. Much as in a real tree, the second layer is expected to capture some of the sunlight that escapes the outer layer through the gaps (Fig. 2). Thus, the second layer can only enhance the amount of sunlight captured, albeit at increased cost. Since the single-layer studies showed that 0° tilt angle of the leaves result in similar performance as leaves tilted at ±20°, it was decided to retain a 0° tilt angle for the outer layer. For the inner layer, two different tilt angles were explored: 0° and 20°. Figure 8 (a) shows the geometry of the double-layered tree and a sample radiation flux distribution for 40° solar incidence angle. It is clear from Fig. 8(b) that the second inner layer of leaves does indeed capture some of the radiation that passes through the gaps in the outer layer. Comparison of the data presented in Table 2 to those in Table 1 clearly shows that a double-layered solar tree, as expected, captures more sunlight. The tilting of the

Table 1. Sunlight captured by a flat panel and a single-layer solar tree under various conditions predicted using Monte Carlo simulations.

Incident Sunlight Angle (θ)	Angle of Tilt of Leaves	Total Sunlight Captured (W)		% Gain(+) or Loss(-) Compared to Flat Panel
		Flat Panel	Solar Tree	
Area Ratio = 1.15 (286 leaves)				
0°	0°	8275 (9516)	3832	-53.69
	±20°		2154	-73.97
	±40°		3235	-60.91
20°	0°	7788 (8956)	5300	-31.95
	±20°		3433	-55.92
	±40°		4375	-43.83
40°	0°	6319 (7267)	6111	-3.29
	±20°		4651	-26.40
	±40°		5172	-18.15
60°	0°	3937 (4528)	6098	+54.89
	±20°		5353	+35.97
	±40°		5420	+37.67
70°	0°	2442 (2808)	5784	+136.86
	±20°		5449	+123.14
	±40°		5275	+116.01
80°	0°	914 (1051)	5272	+476.81
	±20°		5354	+485.78
	±40°		4957	+442.34
Area Ratio = 1.31 (328 leaves)				
0°	0°	8275 (10840)	4390	-46.95
	±20°		5579	-32.58
	±40°		5335	-35.53
20°	0°	7788 (10202)	6080	-21.93
	±20°		6959	-10.64
	±40°		6612	-15.10
40°	0°	6319 (8278)	7013	+10.98
	±20°		7517	+18.96
	±40°		7091	+12.22
60°	0°	3937 (5157)	7008	+78.00
	±20°		7001	+77.83
	±40°		6549	+66.34
70°	0°	2442 (3199)	6646	+172.15
	±20°		6316	+158.64
	±40°		5879	+140.75
80°	0°	914 (1197)	6063	+563.35
	±20°		5401	+490.92
	±40°		4996	+446.61
Area Ratio = 1.54 (384 leaves)				
0°	0°	8275 (12743)	5321	-35.70
	±20°		6150	-25.68
	±40°		5082	-38.59
20°	0°	7788 (11994)	7273	-6.61
	±20°		7820	+0.41
	±40°		6649	-14.63
40°	0°	6319 (9731)	8326	+31.76
	±20°		8568	+35.59
	±40°		7475	+18.29
60°	0°	3937 (6063)	8255	+109.68
	±20°		8133	+106.58
	±40°		7408	+88.16
70°	0°	2442 (3761)	7797	+219.29
	±20°		7450	+205.08
	±40°		6967	+185.30
80°	0°	914 (1408)	7078	+674.40
	±20°		6490	+610.07
	±40°		6313	+590.70

inner leaves appears to have marginal impact on the capture efficiency. In some cases, tilting appears to enhance the capture efficiency, while in others, it does not. Since the single-layer tree with area ratio equal to 1.15 (286 leaves) has more gaps than the one with area ratio equal to 1.54 (384 leaves), it is expected that the improvement manifested by adding a second layer of leaves

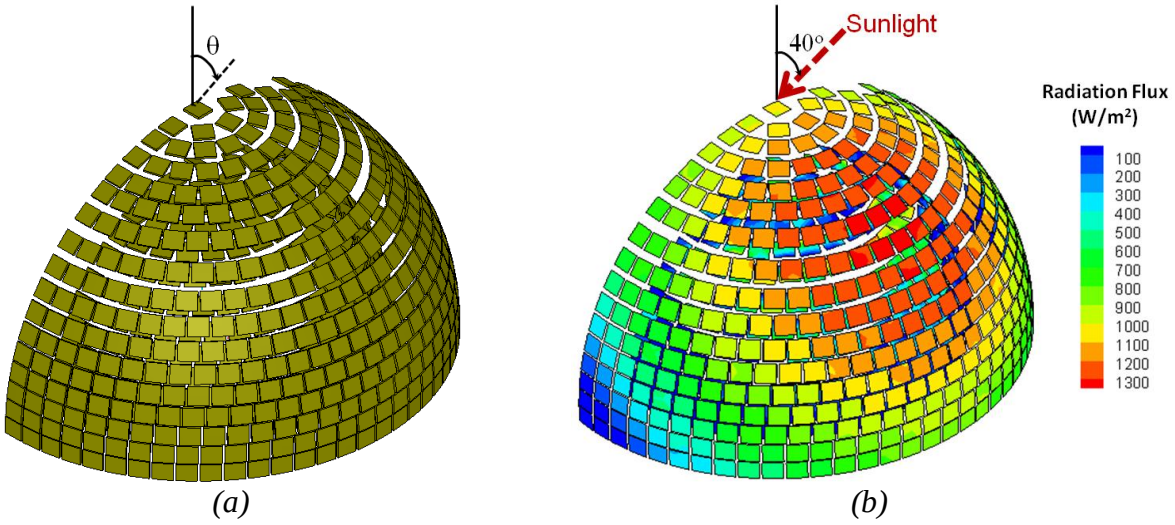

Figure 8. Double-layer solar tree: (a) geometry, (b) computed radiation heat flux with 40^{o} solar incidence angle and leaf tilt angles ranging between $\pm 20^{o}$ for the inner layer only. The incident solar flux is 1362 W/m^2.

would be more pronounced for the smaller area ratio case. A quantitative analysis of the results confirms this contention. Figure 9 shows the improvement in sunlight capture due to the addition of the second inner layer. It is seen that adding the second layer is more beneficial in the case where the outer layer is less dense, i.e., has fewer leaves. The improvement factor increases approximately from 15% for area ratio equal to 1.54 (384 leaves in outer layer) to 30% for area ratio equal to 1.15 (286 leaves in outer layer).

Daily sunlight capture. The preceding studies indicate that solar trees are preferable over flat panels in some cases, but not all. In order to truly compare a solar tree and a flat panel, the transient nature of the solar incidence must be considered, and the sunlight captured must be

Table 2. Sunlight captured by a flat panel and a double-layer solar tree under various conditions predicted using Monte Carlo simulations.

Incident Sunlight Angle (θ)	Angle of Tilt of Panels	Total Sunlight Captured (W)		% Gain(+)/Loss(-) Compared to Flat Panel
		Flat Panel	Solar Tree	
Area Ratio = 1.91 (477 leaves)				
0°	0°	8275	5261	-36.42
	±20°		5592	-32.42
20°	0°	7788	7031	-9.72
	±20°		7225	-7.23
40°	0°	6319	8027	+27.03
	±20°		8113	+28.39
60°	0°	3937	7882	+100.20
	±20°		7810	+98.37
70°	0°	2442	7209	+195.21
	±20°		7078	+189.84
80°	0°	914	6638	+626.26
	±20°		6428	+603.28
Area Ratio = 2.08 (519 leaves)				
0°	0°	8275	5684	-31.31
	±20°		5540	-33.05
20°	0°	7788	7499	-3.71
	±20°		7353	-5.59
40°	0°	6319	8577	+35.73
	±20°		8459	+33.87
60°	0°	3937	8461	+114.91
	±20°		8404	+113.46
70°	0°	2442	7741	+217
	±20°		7700	+215.32
80°	0°	914	7075	+674.07
	±20°		7064	+672.87
Area Ratio = 2.44 (609 leaves)				
0°	0°	8275	6197	-25.11
	±20°		6219	-24.85
20°	0°	7788	8554	+9.84
	±20°		8589	+10.29
40°	0°	6319	9660	+52.87
	±20°		9650	+52.71
60°	0°	3937	9309	+136.45
	±20°		9271	+135.48
70°	0°	2442	8679	+255.41
	±20°		8613	+252.70
80°	0°	914	7785	+751.75
	±20°		7718	+744.42

integrated over a typical day. In an effort to do so, solar incidence angle data was gathered using the solar calculator available from the National Oceanic and Atmospheric Administration (2014). Data was considered for five different cities located at five different latitudes spanning the entire US: Miami (25^{o}N), Los Angeles (34^{o}N), Boulder (40^{o}N), Boston (42^{o}N), and Seattle (47^{o}N). Since the inclination of the sun varies dramatically with seasons, data for the summer and winter solstice were also considered. Figure 10 (a) shows the zenith angle in Boulder (40^{o}N) during

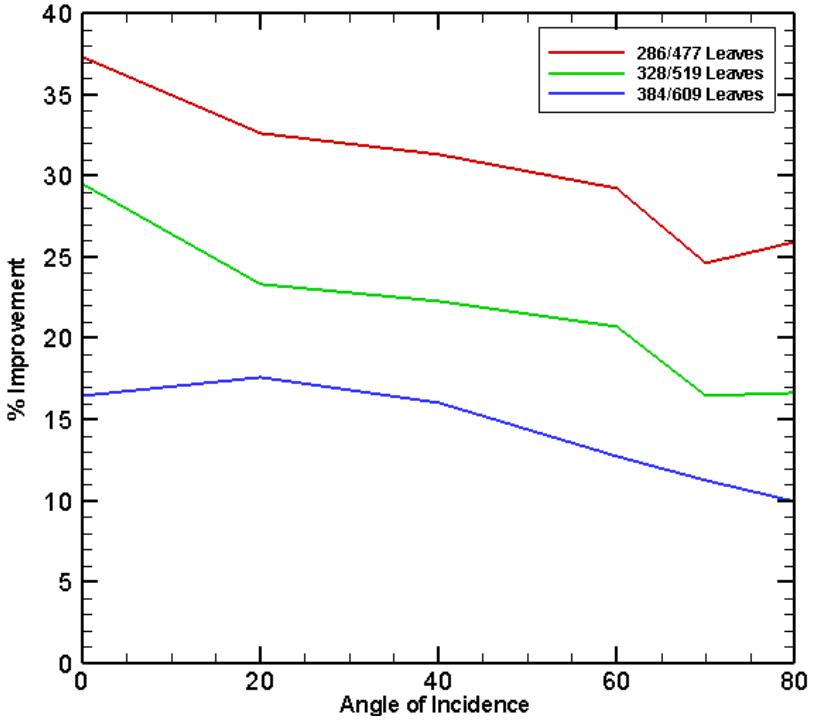

Figure 9. Improvement manifested by adding a second inner layer to the solar tree for various number if leaves in the outer layer. In each case, 191 additional leaves were placed in the second inner layer. For both layers, leaves were not tilted.

different times of the day for both solstices. Figure 10 (b) shows the corresponding sunlight captured by a flat panel and a solar tree under these conditions. The data shown in Fig. 10 (b) was obtained by interpolating the data presented in Table 2 for a double-layered tree with an area ratio of 1.91—the lowest of the three area ratios considered in this study. When integrated from 5 am to 7 pm, the flat panel captures 18,899 Wh, while the solar tree captures 58,369 Wh on the winter solstice. On the summer solstice, the flat panel captures 70,202 Wh, while the solar tree captures 102,887 Wh. Table 3 shows the performance of the solar tree when compared to a flat panel in each of the five cities, as obtained by interpolation of the Monte Carlo data. Substantial gains are predicted for all five cities, with the biggest gains being manifested at high latitudes and in winter.

This analysis demonstrates that irrespective of season, a solar tree is more effective in capturing

Table 3. Daily sunlight capture summary in five different US cities estimated by interpolating data obtained using Monte Carlo simulations.

City	Latitude	Total Sunlight Captured (Wh)					
		Winter Solstice			Summer Solstice		
		Flat Panel	Solar Tree	% Gain Compared to Flat Panel	Flat Panel	Solar Tree	% Gain Compared to Flat Panel
Miami, FL	25°N	33297	72564	**118**	68639	92157	**34**
Los Angeles, CA	34°N	25105	65325	**160**	69562	97592	**40**
Boulder, CO	40°N	18899	58369	**209**	70202	102887	**47**
Boston, MA	42°N	16448	55692	**239**	68576	100376	**46**
Seattle, WA	47°N	11276	47617	**322**	69451	109167	**57**

sunlight, and its effectiveness is dramatically superior to that of a flat panel in winter conditions. It is important to note that in this analysis it is assumed that the solar irradiance is constant throughout the day and is unaltered by atmospheric attenuation. In reality, the solar irradiance is reduced at times of the day far removed from solar noon due to the longer atmospheric path lengths, and therefore, the benefits of a solar tree are somewhat over-predicted by this analysis.

Summary and Conclusions

Traditionally, solar PV cells are assembled as flat panels. These panels must face the sun directly for efficient sunlight capture due to the implications of the cosine law and the fact that the reflectivity of the glass cover on the solar cell increases drastically at shallow (or grazing) angles of incidence. Trees have been designed by nature to capture sunlight efficiently. They overcome the aforementioned barriers by 3D placement of their leaves. No matter what the angle of solar irradiation, some leaves always face the sun directly. Furthermore, by virtue of using the vertical 3D space, the capture area of the leaves on a tree is significantly larger than the 2D footprint area

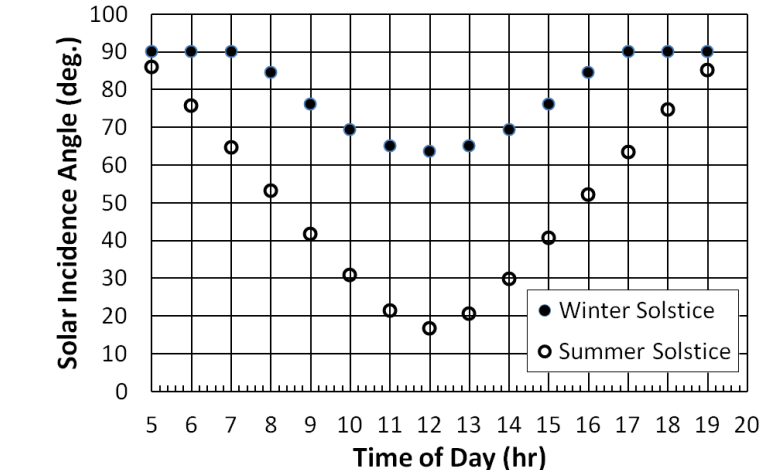

(a)

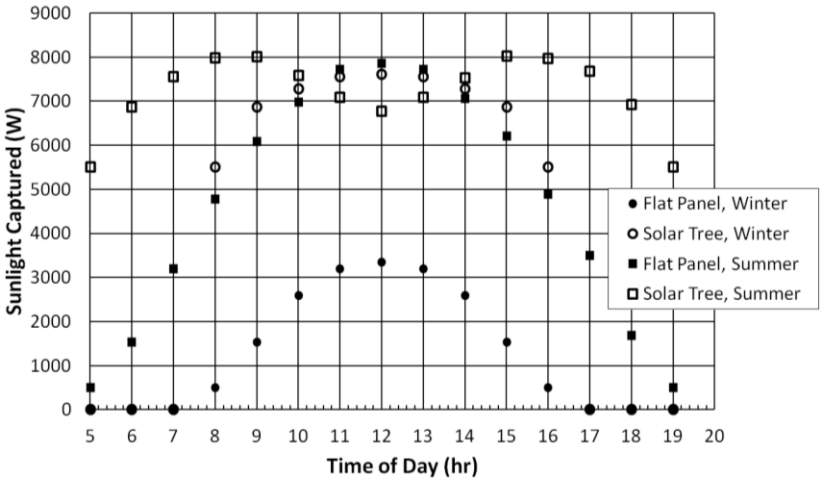

(b)

Figure 10. Daily performance of a flat panel and a double-layered solar tree with area ratio 1.91 situated in Boulder, Colorado (40°N latitude): (a) solar incidence (or zenith) angle, (b) sunlight captured as predicted by Monte Carlo simulations.

of the tree, as indicated by the so-called leaf area index, for which values ranging from 5 to 40 have been reported (Breda, 2003). Thus, even low solar flux densities—as occurring on partly cloudy days—can result in substantial total energy capture.

In this study, high fidelity Monte Carlo simulations of solar radiation transport through treelike structures were conducted. Referred to as solar trees, these structures use solar cells in a configuration mimicking the leaves of a tree. The Monte Carlo simulations were conducted to gain a quantitative understanding of the *pros* and *cons* of a solar tree when compared to

traditional flat panels. First, a tree with a single layer of leaves placed on a hemispherical contour was considered. Studies showed that except for near normal angles of incidence (less than 20^o), solar trees are favorable over flat panels. For angles of incidence above 40^o, solar trees were significantly more efficient than flat panels at capturing sunlight. The gains manifested for shallow angles of incidence of the sun were found to be a factor of five or more, while the losses for normal angle of incidence of the sun were found to be less than 80%. Overall, the variation of the sunlight captured for various angles of incidence was found to be substantially lower for a solar tree than for a flat panel: factor of 3 for a solar tree versus factor of 9 for a flat panel. This implies that a solar tree is a more robust paradigm for capturing sunlight under all conditions than a flat panel. In an effort to mimic leaves of a tree, the solar leaves (cells) were also tilted around their own axes by various amounts. However, no definitive conclusion could be reached with regard to whether this is beneficial for sunlight capture.

In order to further improve the effectiveness of sunlight capture, a second layer of solar leaves were added to the tree, and additional Monte Carlo simulations were conducted. It was found that the second layer of leaves increased the sunlight captured by an additional 15-30% depending on how densely the outer layer is packed. More gains were manifested in cases where the outer layer is less densely packed with leaves since more gaps allow the sunlight to penetrate the outer layer, thereby making the second layer of leaves more worthwhile. As before, tilting of the inner leaves about their own axes did not appear to provide any definitive benefits.

Finally, in order to understand the performance of the solar tree on a daily and seasonal basis, the Monte Carlo results were interpolated to compute the net captured solar radiation during a summer solstice day as well as a winter solstice day in five different cities spanning the entire latitude range of the US. The solar tree manifested maximum gain of 322% in winter and

57% in summer over the flat panel configuration. The biggest gains were manifested in the city with the highest latitude. The results were computed for a solar tree with an area ratio (leaf area index) of only 1.91. Clearly, larger gains would be manifested for larger area ratios. In summary, while some preliminary prototype build-and-test studies have indicated that solar trees may be an effective way of capturing sunlight efficiently, the Monte Carlo simulations performed in this study to quantify the benefits of using a solar tree are the first of their kind, and conclusively demonstrate the benefits of using a tree-like arrangement for solar cells over flat panels.

Acknowledgment

ESI Group is acknowledged for providing licenses to their commercial software CFD-ACE+™.

Nomenclature

A	area of surface element (m^2)
M	total number of surface elements (dimensionless)
n	refractive index (dimensionless)
q_i	radiation flux density on surface i (W/m^2)
Q_i	radiation flux on surface i (W)
R_{ij}	radiation exchange matrix (dimensionless)
T_j	temperature of surface j (K)
δ_{ij}	Kronecker delta function (dimensionless)
ε_j	emissivity of surface j (dimensionless)
ρ	reflectivity (dimensionless)
σ	Stefan-Boltzmann constant (= 5.67×10^{-8} W/m^2 K^4)

References

American Museum of Natural History's Young Naturalist Award Winner's report: http://www.amnh.org/nationalcenter/youngnaturalistawards/2011/aidan.html

Asai, Y., and Toshiaki, Y., (2010), "A Novel Photovoltaic Module Assembled Three Dimensionally," *35th IEEE Photovoltaic Specialists Conference*, Honolulu, HI, June 20 25, 2010, Paper Number 708-V11.

Bartelink, H. H., 1998, "Radiation Interception by Forest Trees: A Simulation Study on Effects of Stand Density and Foliage Clustering on Absorption and Transmission," Ecol. Model., **105**(2,3), pp. 213-225.

Breda, N.J.J., (2003), "Ground-based measurements of leaf area index: a review of methods, instruments, and current controversies," *Journal of Experimental Botany*, Vol. 54(392), pp. 2403-2417

Brown, P. S., and Pandolfo, J. P., 1969, "An Equivalent Obstacle Model for the Computation of Radiative flux in Obstructed Layers," Agricultural Meteorol., **6**(6), pp. 407-421.

Burgermeister, J., (2007), "Introducing the solar tree," available at http://www.renewableenergyworld.com/rea/news/article/2007/12/introducing-the-solar tree-50934

Komp, R.J. (2001), *Practical Photovoltaics: Electricity from Solar Cells*, Aatec Publications, Ann Arbor, Michigan

Lee, R. (1978), *Forest Microclimatology*, Columbia University Press

Mann, J. E., Curry, G. L., and Sharpe, P. J. H., 1979, "Light Interception by Isolated Plants," Agricultural Meteorol., **20**(3), pp. 205-214.

Mazumder, S., (2006), "Methods to Accelerate Ray Tracing in the Monte Carlo Method for Surface-to-Surface Radiation Transport," *Journal of Heat Transfer*, Vol. 128(9), pp. 945 952

Mazumder, S., and Kersch, A., (2000), "A Fast Monte-Carlo Scheme for Thermal Radiation in Semiconductor Processing Applications, *Numerical Heat Transfer*, Part B, vol. 37, no. 2, pp. 185

Mazumder, S., and Ravishankar, M., (2012), "General Procedure for Calculation of Diffuse View Factors between Arbitrary Planar Polygons," *International Journal of Heat and Mass Transfer*, Vol. 55, pp. 7330-7335

Modest, M.F., (2013), *Radiative Heat Transfer*, Third Edition, Academic Press

National Oceanic and Atmospheric Admistration solar calculator, available at http://www.esrl.noaa.gov/gmd/grad/solcalc/azel.html

National Renewable Energy Laboratory website: www.nrel.gov

Palik, E.D., (1997), *Handbook of Optical Constants of Solids*, Elsevier Science

Perttunen, J., Sievannen, R., and Nikinmaa, E., 1998, "LIGNUM: A Model Combining the Structure and the Functioning of Trees," Ecol. Model., **108**(1-3), pp. 189-198.

Verma, L.K., Sakhuja, M., Son, J., Danner, A.J., Yang, H., Zeng, H.C., and Bhatia, C.S., (2011), "Self-cleaning and antireflective packaging glass for solar modules," *Renewable Energy*, Vol. 36, pp. 2489-2493.